ELSEVIER

Carbohydrate Research 279 (1995) 339–352

CARBOHYDRATE RESEARCH

Note

Solution structure of the trisaccharide and hexasaccharide fragments of the O-antigen of the lipopolysaccharide of *Rhizobium tropici* CIAT899

Manuel Bernabé [a], Jesús Jiménez-Barbero [a*], Antonio M. Gil-Serrano [b], Isabel González-Jiménez [b], Pilar Tejero-Mateo [b], Manuel Megías [c]

[a] *Grupo de Carbohidratos, Departamento de Química Orgánica Biológica, Instituto de Química Orgánica, CSIC, Juan de la Cierva 3, 28006 Madrid, Spain*

[b] *Departamento de Química Orgánica, Universidad de Sevilla, Prof. García González s/n, 41071 Seville, Spain*

[c] *Departamento de Microbiología y Parasitología, Facultad de Farmacia, Universidad de Sevilla, Seville, Spain*

Received 10 April 1995; accepted in revised form 18 August 1995

Keywords: Lipopolysaccharide; NMR; Molecular modelling; Conformation; AMBER force field

Surface polysaccharides of Gram-negative bacteria are involved in the molecular mechanism of infections [1]. The chemical structure and primary sequence of the O-antigen of the lipopolysaccharide of *Rhizobium tropici* CIAT899 has been recently analysed by us [2], and has been shown to be formed by the repeating unit

$$\rightarrow 4)\text{-}\beta\text{-D-Glc}p\text{-}(1 \rightarrow 3)\text{-6-deoxy-}\alpha\text{-D-Tal}p\text{-}(1 \rightarrow 3)\text{-}\alpha\text{-L-Fuc}p\text{-}(1 \rightarrow$$

2
↑
OAc

The three-dimensional structure of a carbohydrate is of primary importance to play a role in its biological function [3,4]. On this basis, we now report on the study of the solution conformation of this polysaccharide antigen as well as its corresponding trisaccharide β-D-glucopyranosyl-(1 → 3)-2-*O*-acetyl-6-deoxy-α-D-talopyranosyl-(1 → 3)-L-fucopyranose (**1**) and hexasaccharide β-D-glucopyranosyl-(1 → 3)-6-deoxy-α-D-talopyranosyl-(1 → 3)-α-L-fucopyranosyl-(1 → 4)-β-D-glucopyranosyl-(1 → 3)-6-deoxy-

* Corresponding author. Tel: 91 562 29 00; Fax: 91 562 48 53.

SSDI 0008-6215(95)00300-2

α-D-talopyranosyl-(1 → 3)-L-fucopyranose (**2**) fragments by using NMR spectroscopy and molecular mechanics and dynamics calculations [5].

1. Experimental

NMR experiments.—NMR spectra were recorded at 25°C in D_2O, on a Varian Unity 500 spectrometer. Proton chemical shifts were referenced to residual HDO at δ 4.76. Carbon chemical shifts were referenced to external dioxane at δ 67.4. The DQF-COSY experiments were performed in the phase sensitive mode using the standard Varian sequence [6]. A data matrix of 256 * 2 K complex points was used to digitize a spectral width of 4500 Hz. 16 scans were used per increment with a relaxation delay of 2 s. The 90° pulse width was 7.5 μs. Prior to Fourier transformation, zero filling was used in F_1 to expand the data to 1 K * 2 K. The pure absorption one bond proton–carbon correlation experiments were collected in the ^{1}H-detection mode using the HMQC pulse sequence [7] and a reverse probe. A data matrix of 256 * 2 K complex points was used to resolve a spectral width of 10,000 Hz and 4500 Hz in F_1 and F_2, respectively. 16 scans were used per increment with a relaxation delay of 2 s and a delay corresponding to a J value of 152 Hz. A BIRD-pulse was used to minimize the proton signals bonded to ^{12}C. ^{13}C-decoupling was achieved by the WALTZ scheme. Squared cosine bell functions were applied in both dimensions and zero filling was used in F_1 to expand the data to 2 K * 2 K. The HMBC experiment [8] was recorded using a similar pulse sequence with 96 scans, removing the BIRD module, using a low J-pass filter, and with no decoupling during acquisition. A delay of 80 ms was used for evolution of long range couplings. Squared cosine bell functions were applied in both dimensions, and zero filling in F_1 to expand the data to 2 K * 2 K. The 2D rotating frame NOE (ROESY, CAMELSPIN) experiments [9] were recorded in the phase sensitive mode. The spin-lock period consisted of a train of 30° pulses (2.5 μs), separated by delays of 50 μs. Therefore, the spin locking field amounts to 1700 Hz. The total mixing time was set to 250–600 ms. The rf carrier was set at δ 6.0 ppm to minimize spurious Hartmann–Hahn effects [10]. A data matrix of 256 * 2 K complex points was used to resolve a spectral width of 4500 Hz. 32 scans were used per increment with a relaxation delay of 2 s. Prior to Fourier transformation, squared sine bell functions shifted by $\pi/2$ were applied in both dimensions and zero filling was used in F_1 to expand the data to 2 K * 2 K. The spectrum was integrated using standard Varian software after applying a third order polynomial baseline correction in F_2. The ROESY intensities were corrected according to their corresponding offset. The cross peaks intensities were estimated to have a ±15% of error. Different protocols were employed to estimate the cross relaxation rates, and therefore, interproton distances, from the rotating frame experiments. (a) For a given mixing time, the total intensity of the added F_1 cross sections containing diagonal and cross-peaks was given a 100% value [11]. (b) By extrapolation to zero mixing time of the linear dependence of $2I_{ij}/(I_{ii} * \text{mixing time})$ versus mixing time, where I_{ij} and I_{ii} are the integrated volumes of the cross peaks and diagonal peaks, respectively [12]. (c) By using the ratio [13] $x = I_{ij}/I_{ii}$ according to the equations, $Rc = (k/\text{mixing time})$ $\ln[(1+x)/(1-x)]$, where $k = 1$ if $\omega\tau_c \gg 1$ and $k = -1$ if $\omega\tau_c \ll 1$ [14]. The 2D

NOESY experiment [15] was recorded in the phase-sensitive mode with a mixing time of 300 ms. A data matrix of 256 * 2 K complex points was used to resolve a spectral width of 4500 Hz. 32 scans were used per increment with a relaxation delay of 2 s. A similar processing to that described for ROESY was applied.

Molecular mechanics and dynamics calculations.—Glycosidic torsion angles are defined as Φ_H H-1′–C-1′–O-1′–C–X, Ψ_H C-1′–O-1′–C–X–H–X. Disaccharide entities are abbreviated as Glc–Tal, Tal–Fuc, and Fuc–Glc, for β-D-glucopyranosyl-(1 → 3)-2-*O*-acetyl-6-deoxy-α-D-talopyranose, 6-deoxy-α-D-talopyranosyl-(1 → 3)-α-L-fucopyranose, and α-L-fucopyranosyl-(1 → 4)-β-D-glucopyranose, respectively. Relaxed residue (Φ,Ψ) potential energy maps were calculated for all the disaccharide entities of **1** and **2** by using the AMBER force field parametrised for carbohydrates by Homans [16]. The previous step involved the generation of the corresponding rigid residue maps by using a grid step of 12°. Then, every Φ, Ψ point of this map was optimised using 200 steepest descent steps, followed by 1000 conjugate gradient iterations. Following this protocol, the maximum rms derivative in low energy regions was smaller than 0.05 kcal/mol*Å. Despite the restriction set around the glycosidic linkages (2500 kcal/mol/rad^2), deviations smaller than 0.3° in Φ, Ψ values were observed in high energy regions. This high restriction was used in order to keep the Φ, Ψ values at the desired position. Only the *gg* conformation of the lateral chain was used for the glucose residue [17]. The starting position for the secondary hydroxyl groups was set as *rr* (anti-clockwise). A dielectric constant of 78 D was used for the calculations. Populations were derived using a Boltzmann distribution from the AMBER steric energy values. The combination of the global minima found for the constituent disaccharide entities were used to build the trisaccharide and hexasaccharide structures, **1** and **2**, which were subsequently minimized in an exhaustive way. These geometries were then taken as starting structures for Molecular Dynamics calculations in vacuo by using the AMBER force field as integrated in the Discover 2.9 program [18]. The MD simulations were performed at 300°K with dielectric constants of 78 D, and a time step of 1 fs. The equilibration time was set to 150 ps while the total simulation time was 750 ps. The temperature was controlled during the equilibration and simulation periods by coupling to a temperature bath, using an exponential decay constant of 0.1 ps [19]. During the equilibration, the velocities were rescaled when the difference between the actual and the required temperature was higher than 10°. Trajectory frames were saved every 1 ps. The trajectories were then examined with the Analysis module of INSIGHT II [20]. $\langle r^{-6} \rangle$ distances were also calculated using the Analysis module. The polysaccharide was built from the corresponding disaccharide entities, using the global minima for every glycosidic linkage.

2. Results and discussion

Table 1 shows the values of the steric energies of the different conformers of the constituent disaccharide entities (Glc–Tal and Tal–Fuc) of trisaccharide **1**, obtained, as described in Experimental, by using the AMBER force field parametrised by Homans for carbohydrate molecules [16].

Table 1
Relevant interatomic distances and steric energy differences (kcal/mol) for the relevant low energy conformers of the disaccharide entities of oligosaccharides **1** and **2**. Φ/Ψ are rounded values

Glycosidic linkage	Glc–Tal		Tal–Fuc			Fuc–Glc	
Parameter	Conformer						
	A	B	C	D	E	F	G
Φ/Ψ	50/10	180/0	−60/0	−40/−160	60/10	−50/−40	70/30
$r_{H\text{-}1'-H2}$	2.6	4.1	3.8	1.9	4.5	4.0	5.3
$r_{H\text{-}1'-H4}$	4.1	4.1	4.1	3.6	2.8	3.0	2.7
$r_{H\text{-}1'-H3}$	2.2	3.4	2.4	3.3	2.5	2.5	4.5
$r_{H\text{-}1'-H5}$	4.8	5.8	4.9	4.5	4.3	4.4	3.3
$r_{H\text{-}5'-H4}$	4.9	5.9	1.8	5.2	5.2	4.4	2.4
Energy	0.0	1.1	0.0	3.1	4.1	0.0	3.6

Relaxed energy plots of the isoenergy contours are given in Fig. 1. It can be observed that both adiabatic maps show a similar shape, although the surface of Glc–Tal seems to be more extended along both Φ, Ψ axes. This fact is reasonable, in principle, since the site of attachment of the glycosidic linkage to the talose moiety shows two axial oxygen substituents, while that to fucose has only one equatorial and one axial. Therefore, according to the observations previously reported [21] by Anderson et al., a higher rigidity along the Ψ angle for Tal–Fuc is to be expected. The lowest energy region (below 5 kcal/mol from the global minimum) of Glc–Tal is described by glycosidic torsion angles $\Phi = 50 \pm 30$, $\Psi = 0 \pm 65°$ (global minimum at ca. 50/10), and interproton distance $r_{H\text{-}1'-H\text{-}3} = 2.2 \pm 0.4$ Å, appears to be populated to greater than 90%, while there is a small island centered about 180/0°, which is populated less than 5% at 40°. For Tal–Fuc, the corresponding low energy region is described by torsion angles $\Phi = -50 \pm 20$, $\Psi = -10 \pm 55°$ (global minimum at ca. −60/0), and interproton distance $r_{H\text{-}1'-H\text{-}3} = 2.4 \pm 0.4$ Å and is populated to greater than 95%. The rest of the

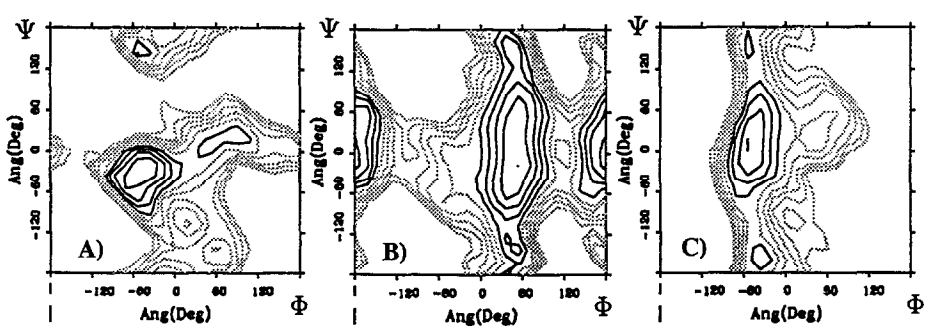

Fig. 1. Relaxed energy maps of the isoenergy contours (1 kcal/mol) obtained by using AMBER ($e = 80$) for the disaccharide entities of the O-antigen of the polysaccharide of *Rhizobium tropici* CIAT899. (A) Fuc–Glc, (B) Glc–Tal, and (C) Tal–Fuc.

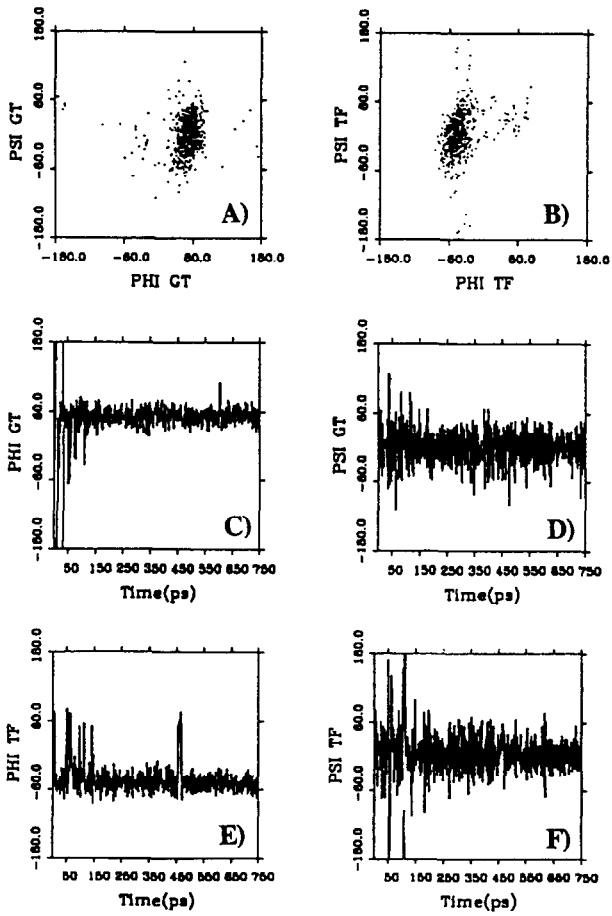

Fig. 2. Trajectory plots of the MD simulation (AMBER, $\varepsilon = 80$, time 750 ps) of trisaccharide 1. (A) Trajectory of the simulation in Φ/Ψ space for Glc–Tal. (B) Trajectory of the simulation in Φ/Ψ space for Tal–Fuc. (C) History of Φ of Glc–Tal. (D) History of Ψ of Glc–Tal. (E) History of Φ of Tal–Fuc. (F) History of Ψ of Tal–Fuc.

population derives from this region towards positive Φ angles. It has to be noted that all these populations are calculated from steric energy values which correspond to enthalpies and not to true free energies.

As a further step, one structure of **1** was built from the global minima of both maps and after extensive minimization, its conformational stability was studied by using molecular dynamics simulations with the DISCOVER-AMBER program. The trajectories of the glycosidic linkages are displayed in Fig. 2. In all cases, no chair-to-chair or chair-to-boat interconversions were observed. For Glc–Tal, the average Φ/Ψ angles were calculated to be 50/10, while for Tal–Fuc, the corresponding values were $-50/0$. It can be observed that the trajectories remained for most of the time ($> 90\%$) in the low energy regions previously mentioned.

Table 2
^{1}H-NMR chemical shifts (∂, ppm) and coupling for trisaccharide **1**, hexasaccharide **2**, and the O-antigen of the lipopolysaccharide of *Rhizobium tropici* CIAT899

Unit	H-1	H-2	H-3	H-4	H-5	H-6a	H-6b
Trisaccharide **1**							
α-L-Fuc*p* [a]	5.21	3.87	3.89	3.87	4.21	1.19 [d]	–
2-*O*-Ac-6-d-α-D-Tal*p*	5.12	5.35	4.40	3.95	4.21	1.26 [d]	–
β-D-Glc*p*	4.60	3.31	3.49	3.41	3.45	3.73	3.90
β-L-Fuc*p* [b]	4.59	3.54	3.69	3.80	3.81	1.23 [d]	–
Hexasaccharide **2**							
α-L-Fuc*p* [a]	5.21	3.90	3.90	3.88	4.22	1.19 [d]	–
6-d-α-D-Tal*p*	5.14	4.15	4.18	3.96	4.16	1.26 [d]	–
β-D-Glc*p* [c]	4.67	3.42	3.50	3.44	3.45	3.73	3.89
β-L-Fuc*p* [b]	4.60	3.53	3.69	3.80	3.82	1.23 [d]	–
α-L-Fuc*p*	4.97	3.88	3.90	3.88	4.42	1.17 [d]	–
β-D-Glc*p*	4.69	3.40	3.57	3.56	3.64	3.85	3.95
Polysaccharide							
6-d-α-D-Tal*p*	5.11	4.15	4.17	3.95	4.16	1.25 [d]	–
α-L-Fuc*p*	4.96	3.88	3.89	3.87	4.41	1.26 [d]	–
β-D-Glc*p*	4.67	3.41	3.56	3.56	3.63	3.84	3.94

[a,b] Reducing ends;
[c] Non-reducing end;
[d] Protons of C-6 methyl group.

NMR spectroscopy can be used to distinguish the presence of either conformer [22]. The low energy region for Tal–Fuc has short distances between Fuc–H-3 and Tal–H-1′, and Fuc–H-4 and Tal–H-5′, while that for Glc–Tal shows close contacts between Tal–H-3 and Glc-H-1′. The area within the low energy region with positive Ψ torsion angles also bring Tal–H-2 and Glc–H-1 into close proximity. These structural characteristics are also shown in Table 1. The observation of one or two interresidue NOEs can impose constraints in the potential energy map to verify the existence of a given conformation [23]. The previous step for the analysis of the NOE data was the assignment of the different resonances as described through a combination of 2D-NMR COSY, TOCSY, HMQC and HMBC techniques [2]. The first-order chemical shifts for **1** are shown in Table 2.

Hydroxymethyl conformation.—Glc $H6_{proR}$ and $H6_{proS}$ were assigned as previously reported [17,24]. The distribution of rotamers was calculated, following well established methodology, assuming a *gt*: *gg* equilibrium. The observed couplings (2.4, 5.4 Hz) agree with combinations of the *gt* and *gg* rotamers, with the *gg* family populated to an extent of ca. 60%.

Analysis of NOE data.—The conformational analysis of oligosaccharide structures based on NOE data has been performed in several ways [25]. In this case, rotating-frame NOE experiments (Fig. 3) were used to obtain the experimental interproton distances, since the corresponding NOESY maps did not show relevant cross peaks, an indication of a molecule with $\omega\tau_c$ ca. 1.1 [9,14,25]. Qualitatively, the existence of NOEs between

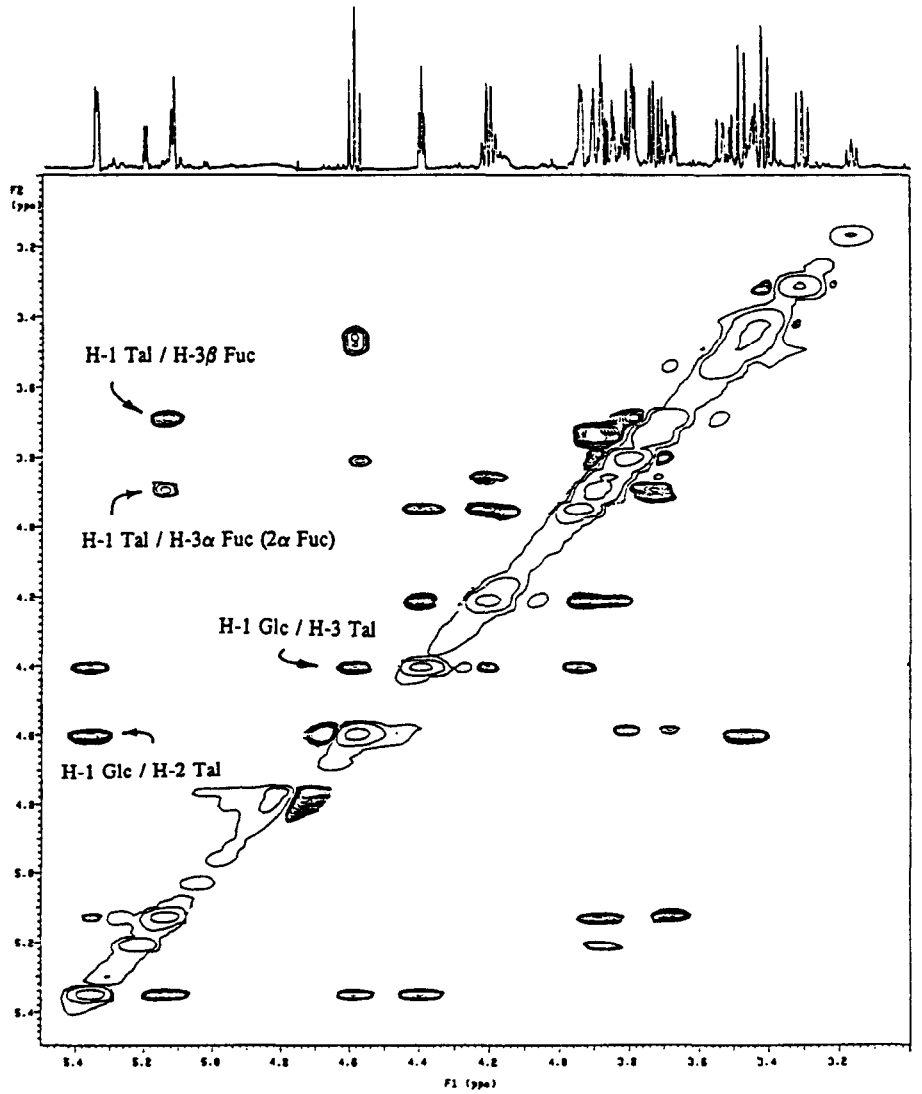

Fig. 3. ROESY spectrum (300 ms) of **1** in D_2O at 300 K. Relevant cross-peaks are indicated. Cross peaks have the opposite sign to the diagonal peaks.

Glc–H-1 and Tal–H-3 and between Tal–H-1 and Fuc–H-3 implies that the glycosidic angles of compound **1** spend most of its time within the calculated low energy regions. On the other hand, the relevant Glc–H-1–Tal–H-2 NOE indicates that the region defined by positive Ψ angles is strongly populated in water solution. The corresponding average distances for Glc–H-1–Tal–H-2, Glc–H-1–Tal–H-3, and Glc–H-1–Tal–H-4 proton pairs from MD simulations are 3.15 Å, 2.50 Å, and 4.10 Å, respectively, although oscillations could be observed. On the other hand, the calculation of $\langle r^{-6} \rangle$

Table 3
Calculated (from MD simulations) and experimental (ROESY) distances for the relevant interresidue proton pairs of compounds **1** and **2** in D_2O. Experimental distances are based on cross peak intensities, assuming a rigid isotropic tumbling molecule. Cross peak intensities were assumed to have a ±15% error. Distances for the hexasaccharide are only approximated and should be regarded with caution, since the key protons present overlapping

Proton pair	Distance	
	MD	ROESY
Glc-H-1/Tal-H-2	2.87	2.3–2.5
Glc-H-1/Tal-H-3	2.40	2.4–2.6
Glc-H-1/Tal-H-4	3.43	3.5–4.0
Fuc-H-1/Tal-H-4	3.43	3.5–4.0
Fuc-H-1/Glc-H-4	3.20 [a]	3.1–3.7 [b]
Tal-H-1/Fuc-H-2	3.59/3.42 [a]	3.2–4.0
Tal-H-1/Fuc-H-3	2.35/2.43 [a]	2.2–2.6
Tal-H-1/Fuc-H-4	3.38/3.17 [a]	3.2–4.0
TAl-H-5/Fuc-H-4	2.15	2.2–2.5 [b]

[a] MD of the hexasaccharide **2**.
[b] Approximated values due to partial overlapping.

averaging for the same simulation provides the values to be compared to the NOE results [14,26]. These are 2.87, 2.40, and 3.43, respectively (Table 3). According to these values, besides those observed NOEs, we could also expect the presence of a small NOE between Glc–H-1–Tal–H-4 protons. In fact, this NOE can be detected at the noise level. For the Tal–Fuc glycosidic linkage, the $\langle r^{-6} \rangle$ values are 3.59, 2.35, and 3.38 Å, for Tal–H-1–Fuc–H-2, Tal–H-1–Fuc–H-3, and Tal–H-1–Fuc–H-4 proton pairs, respectively. The corresponding Tal–H-5–Fuc–H-4 distance is 2.15 Å. The experimental distances were estimated from the ratio of the integrated cross peak volumes of the ROESY experiment. Intraresidue Tal–H-1–Tal–H-2 and Tal–H-2–Tal–H-3 cross peaks were used as references. Taking into account the cross relaxation rates obtained by the different protocols (see Experimental), and the estimated error for the cross peak intensities, the actual distances for the Glc–Tal unit would range for Glc–H-1–Tal–H-2 between 2.3–2.5 Å, Glc–H-1–Tal–H-3 2.4–2.5 Å, and Glc–H-1–Tal–H-4 3.5–4.0 Å, while those for the Tal–Fuc moiety are Tal–H-1–Fuc–H-2 3.4–4.0 Å, Tal–H-1–Fuc–H-3 2.2–2.6 Å, Tal–H-1–Fuc–H-4 3.4–4.0 Å, and Tal–H-5–Fuc–H-4 2.2–2.5 Å. There is some uncertainty in the obtained distances due to the partial overlapping of Fuc–H-3 and –H-4, and Fuc–H-5 and Tal–H-5 proton resonances. Nevertheless, the comparison among the observed and expected interresidue cross peaks indicates that a satisfactory match could be obtained by considering the presence of flexibility around the global minimum for both glycosidic linkages as calculated by the MD simulations for **1**. The only small discrepancy appears for Glc–H-1–Tal–H-2, for which the experimental distance is smaller than that calculated by the simulations. According to the experimental NOEs, this glycosidic linkage seems to spend more time in the region with positive Ψ angles. In addition, according to the experimental data, the presence of other conformers (> 5%) can be discarded. Therefore, according to our results, the AMBER force field [16], when used in these conditions (bulk and high dielectric

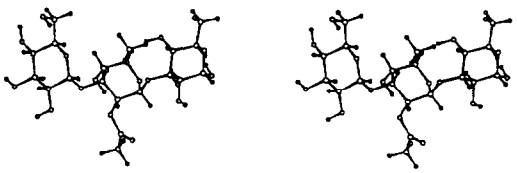

Fig. 4. Stereoscopic view of the global minimum of **1**, obtained from MM and MD simulations and NOE experiments.

constant), does satisfactorily reproduce the conformational properties of **1**. Therefore, at least for this particular case, it does not seem necessary to include the experimental NOE constraints in the MD simulation as recently indicated by the group of Homans [27].

These results indicate that the extent of flexibility around the glycosidic linkages of **1** in water solution is rather limited, and that less than 10% of the complete potential energy surfaces are populated in solution. Compound **1** shows a moderate flexibility, similar to that proposed for different oligosaccharide molecules [28].

A view of the global minima of **1** is shown in Fig. 4. The superimposition of different conformers found in the simulation (data not shown) indicates that the global shape of the Fuc and Tal pyranoid rings is very similar, while the Glc moiety shows higher fluctuations.

Hexasaccharide **2**.—Trisaccharide **1** is the repeating unit of the O-antigen of a lipolysaccharide which also includes an additional α-L-Fuc–(1 → 4)-Glc linkage [2]. An hexasaccharide fragment has also been obtained by partial hydrolysis [2] of this polysaccharide. The proton chemical shifts for this hexasaccharide **2** are also given in Table 2. The most relevant variation with regard to **1** is the lack of the 2-*O*-acetyl group at the Tal moiety. A similar approach to that described above was employed to study the tri-dimensional structure of **2**. The relaxed energy map for the remaining glycosidic linkage, Fuc–Glc, is also presented in Fig. 1. A hexasaccharide molecule was built from the global minima of **1** and α-L-Fuc–(1 → 4)-Glc, which, after extensive minimization, was also submitted to AMBER MD simulations in vacuo ($\varepsilon = 78$). The trajectories of the different linkages during 500 ps are shown in Fig. 5. The average Φ/Ψ angles and the corresponding distances (from $\langle r^{-6} \rangle$ averaging) are also gathered in Table 3. As expected, the results for the Tal–Fuc and Glc–Tal linkages are remarkably similar to those described above for **1**, while Fuc–Glc shows certain flexibility, mainly around angle Ψ. Although there is a short incursion (ca. 100 ps) to the positive Φ region for the Tal–Fuc glycosidic linkage, the trajectory goes back to the main low energy region and stays there for the rest of the simulation. This slightly higher flexibility of the Tal–Fuc moiety may be due to the lack of the 2-*O*-acetyl moiety of the talopyranosyl residue in the hexasaccharide. It can be observed that this incursion into the positive Φ region does not substantially modify the ensemble average distances (calculated from $\langle r^{-6} \rangle$ values) in comparison with those calculated for the trisaccharide and even with the global minima of **1** and **2**. Therefore, the simulation should be regarded as one of the possible distributions which is in agreement with the limited (see below) NOE data. The modelling results are in agreement with an independent behaviour for every glycosidic linkage of both **1** and **2**, as is usually observed in small linear oligosaccharides. In fact,

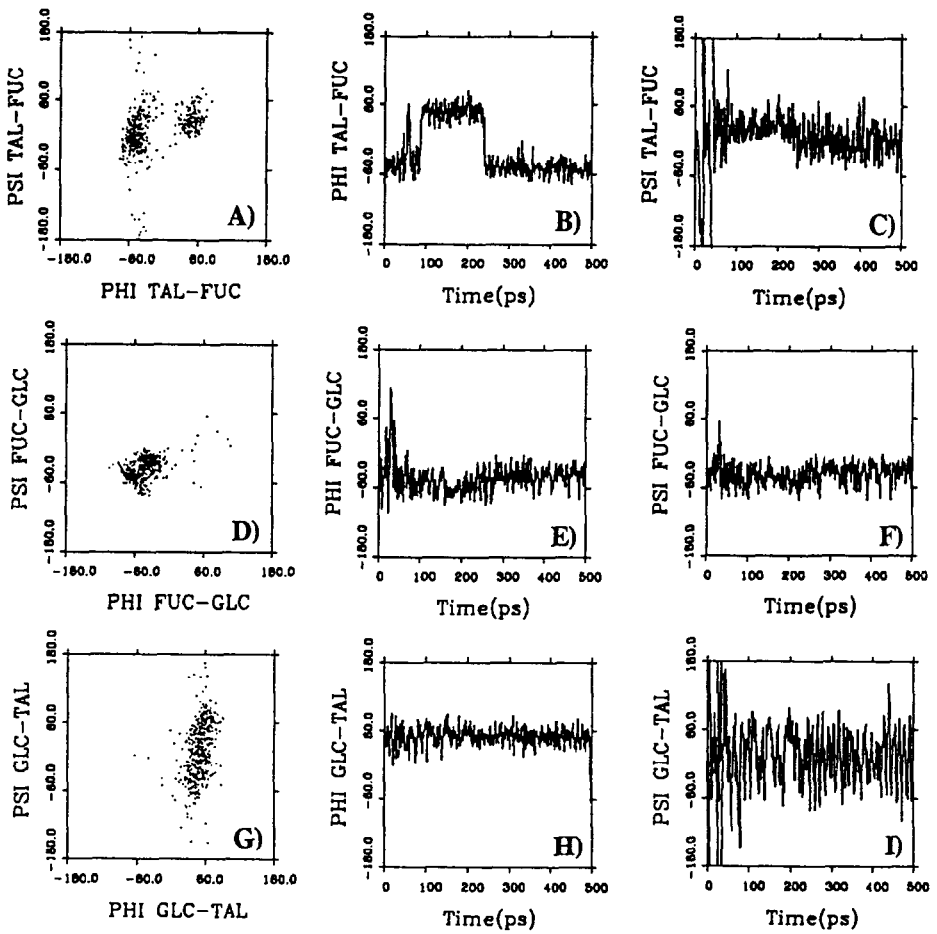

Fig. 5. Trajectory plots of the MD simulation (AMBER, $\varepsilon = 80$, time 500 ps) of hexasaccharide **2**. (A) Trajectory of the simulation in Φ/Ψ space for Tal–Fuc. (B) History of Φ of Tal–Fuc. (C) History of Ψ of Tal–Fuc. (D) Trajectory of the simulation in Φ/Ψ space for Fuc–Glc. (E) History of Φ of Fuc–Glc. (F) History of Ψ of Fuc–Glc. (G) Trajectory of the simulation in Φ/Ψ space for Glc–Tal. (H) History of Φ of Glc–Tal. (I) History of Ψ of Glc–Tal.

no experimental NOEs were found between non-connected residues. Although the overlapping and strong coupling of the key protons in the NMR ROESY spectra of **2** precludes a quantitative analysis of the NOE data, the comparison between the expected and the observed ROESY contacts (Fig. 6) seems to show again a satisfactory agreement between the NMR data and the calculations employing AMBER. Again, the superimposition of different conformers found in the MD simulation indicates that there are potential fluctuations around the glycosidic linkages of the hexasaccharide, although the global shape of the chain remains basically the same.

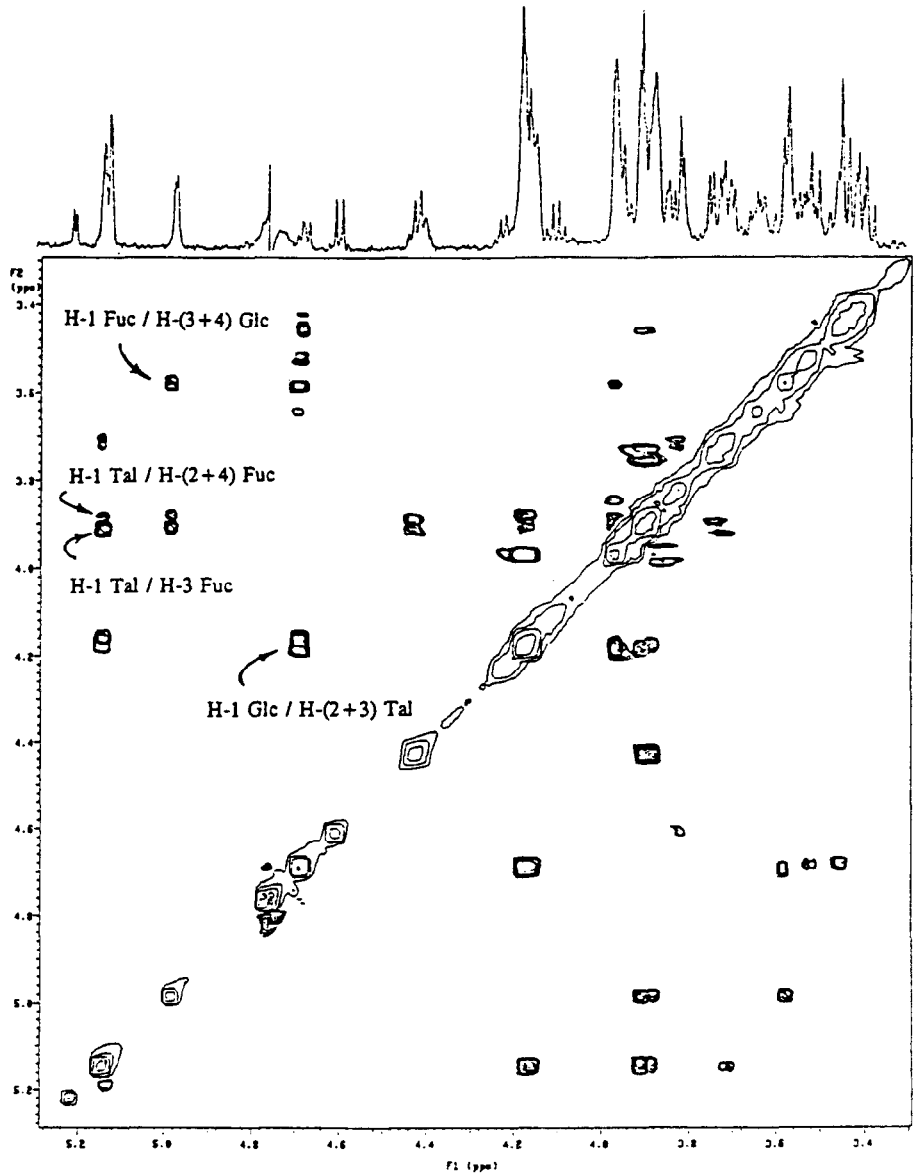

Fig. 6. ROESY spectrum (250 ms) of **2** in D_2O at 300 K. Relevant cross-peaks are indicated. Cross peaks have opposite sign than the diagonal peaks.

Finally, a polysaccharide structure was built from the global minima of the different glycosidic linkages. As observed for the hexasaccharide, the overlapping signals make a quantitative analysis difficult. Nevertheless, the observed NOESY cross peaks for the

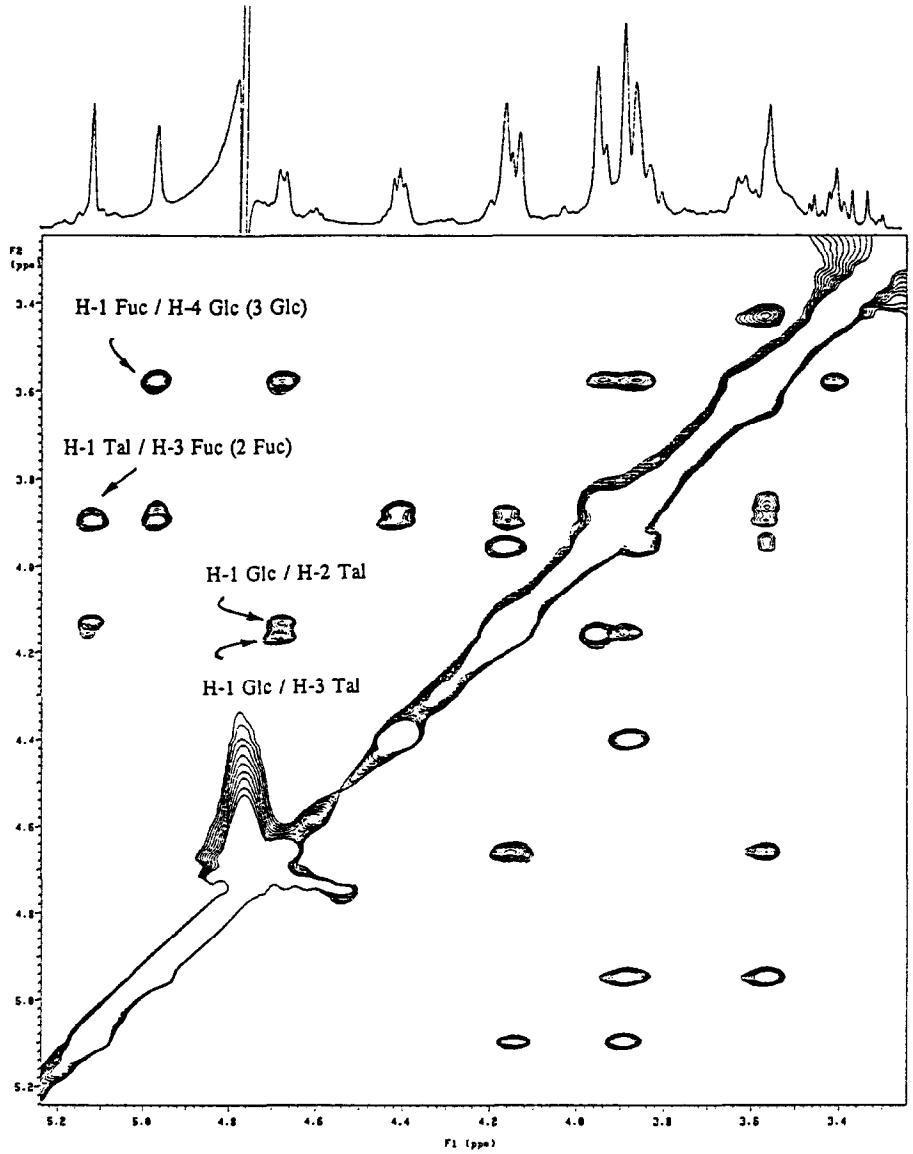

Fig. 7. NOESY spectrum (300 ms), in D_2O at 300 K, of the O-antigen of the polysaccharide of *Rhizobium tropici* CIAT899. Relevant cross-peaks are indicated. Cross peaks have the same sign than the diagonal peaks.

complete polysaccharide (Fig. 7) are also in agreement with a large conformational population around the previously described minima for the different glycosidic linkages of **1** and **2**. Therefore, this structure can be considered to be representative of the complete O-antigen of the lipopolysaccharide of *Rhizobium tropici* CIAT899 [2] (Fig.

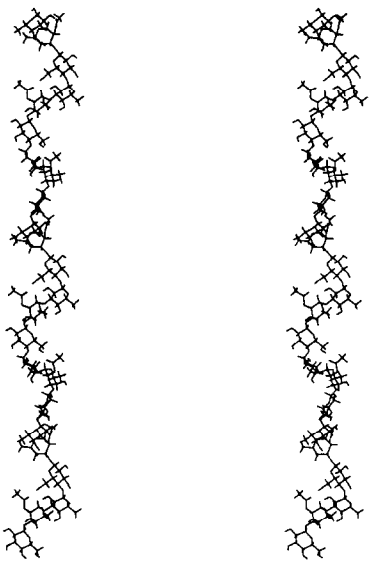

Fig. 8. Stereoscopic view of the structure of the O-antigen of the polysaccharide of *Rhizobium tropici* CIAT899, built from the global minima found for every glycosidic linkage. A helical-type form with repeating block of nine residues may be observed.

8). It can be observed that the polysaccharide tends to adopt a helical form, in which the repeating block corresponds to nine residues.

Acknowledgements

We thank DGICYT (grants PB-93-0127 and BIO093-0716-C04-03) for financial support, and the Fundación Cámara for the grant of a fellowship to one of the authors (I.G.-J.).

References

[1] (a) R.A. Brink, J. Miller, R.W. Carlson, and K.D. Noel, *J. Bacteriol.*, 172 (1990) 548–555. (b) R. Carlson, R. Shatters, J. Duh, E. Turnbull, B. Hanley, B. Rolfe, and M. Djordjevic, *Plant Physiol.*, 84 (1987) 421–427. (c) R.W. Carlson, S. Kalembasa, D. Turowski, P. Pachori, and K.D. Noel, *J. Bacteriol.*, 169 (1987) 4923–4928. (d) R.A. de Maagd, A.S. Rao, I.H.M. Mulders, L. Goosen de Roo, M.C.M. van Loosdrecht, C.A. Wijffelman, and B.J.J. Lugenberg, *J. Bacteriol.*, 171 (1989) 1143–1150. (e) U.B. Priefer, *J. Bacteriol.*, 171 (1989) 6161–6168.

[2] A.M. Gil-Serrano, I. González-Jiménez, P. Tejero-Mateo, M. Bernabé, J. Jiménez-Barbero, M. Megías, and M.J. Romero-Vazquez, *Carbohydr. Res.*, 275 (1995) 285–294.

[3] (a) K.G. Rice, P. Wu, L. Brand, and Y.C. Lee, *Curr. Opin. Struc. Biol.* 3 (1993) 669–674. (b) C.A. Bush, *Curr. Opin. Struc. Biol.* 2 (1992) 655–660.

[4] Y. Bourne, H. van Tielbeurgh, and C. Cambillau, *Curr. Opin. Struc. Biol.*, 3 (1993) 681–686.

[5] A.D. French and J.W. Brady (Eds.), *Computer Modelling of Carbohydrate Molecules*, ACS Symp. Ser. 430, American Chemical Society, Washington, DC, 1990.
[6] U. Piantini, O.W. Sorensen, and R.R. Ernst, *J. Am. Chem. Soc.*, 104 (1982) 6800–6801.
[7] A. Bax and S. Subramanian, *J. Magn. Reson.*, 67 (1986) 565–569.
[8] A. Bax and M.F. Summers, *J. Am. Chem. Soc.*, 108 (1986) 2093–2094.
[9] A.A. Bothner-By, R.L. Stephens, J.-M. Lee, C.D. Warren, and R.W. Jeanloz, *J. Am. Chem. Soc.*, 106 (1984) 811–813.
[10] A. Bax and D.G. Davis, *J. Magn. Reson.*, 63 (1985) 207–213.
[11] J. Breg, L.M.J. Kroon-Batenburg, G. Strecker, J. Montreuil, and J.F.G. Vliegenthart, *Eur. J. Biochem.*, 178 (1989) 727–739.
[12] H. van Halbeek and L. Poppe, *Magn. Reson. Chem.*, 30 (1992) S74–S86.
[13] G. Bodenhausen and R.R. Ernst, *J. Am. Chem. Soc.*, 104 (1982) 1304–1305.
[14] G. Esposito and A. Pastore, *J. Magn. Reson.*, 76 (1988) 331–336.
[15] (a) D. Neuhaus and M.P. Williamson, *The Nuclear Overhauser Effect in Structural and Conformational Analysis*, VCH Publishers, New York, 1989. (b) J.H. Noggle and R.E. Schirmer, *The Nuclear Overhauser Effect: Chemical Applications*, Academic Press, New York, 1971.
[16] S.W. Homans, *Biochemistry*, 29 (1990) 9110–9118.
[17] L.M.J. Kroon-Batenburg and J. Kroon, *Biopolymers*, 29 (1990) 1243–1248.
[18] Discover 2.9.5 Program. Biosym Technol. Inc., San Diego, USA.
[19] H.J.C. Berendsen, J.P.M. Postma, W.F. van Gunsteren, A. Di Nola, and J.R. Haak, *J. Chem. Phys.*, 81 (1984) 3684–3690.
[20] Insight II 2.3.0. Program. Biosym Technol. Inc., San Diego, USA.
[21] J.E. Anderson and D.G. Watson, *J. Am. Chem. Soc.*, 114 (1992) 1517–1518.
[22] C.A. Bush and P. Cagas, *Adv. Biophys. Chem.*, 2 (1992) 149–180.
[23] (a) K. Bock, *Pure Appl. Chem.*, 55 (1983) 605–622. (b) B. Meyer, *Top. Curr. Chem.*, 154 (1990) 141–208.
[24] Y. Nishida, H. Hori, H. Ohrui, and H. Meguro, *J. Carbohydr. Chem.*, 7 (1988) 239–250.
[25] (a) J.R. Brisson and J.P. Carver, *Biochemistry*, 26 (1983) 6664–6676. (b) K.E. Miller, C. Mukhopadhyay, P. Cagas, and C.A. Bush, *Biochemistry* 26 (1990) 6703–6709, and references therein. (c) K. Bock, H. Lönn, and T. Peters, *Carbohydr. Res.*, 198 (1990) 375–380.
[26] (a) D.A. Cumming and J.P. Carver, *Biochemistry*, 26 (1987) 6664–6676. (b) J.P. Carver, S.W. Michnick, A. Imberty, and D.A. Cumming, *Carbohydrate Recognition in Cellular Function*, CIBA Foundation Symp. 145, Wiley, New York, pp 6–26. (c) J.P. Carver, *Pure Appl. Chem.*, 65 (1993) 763–770. (d) A. Imberty, V. Tran, and S. Perez, *J. Comput. Chem.*, 11 (1989) 205–216.
[27] T.J. Rutherford, J. Partridge, C.T. Weller, and S.W. Homans, *Biochemistry*, 32 (1993) 12715–12724.
[28] M. Hricovini, R.N. Shah, and J.P. Carver, *Biochemistry*, 31 (1992) 10018–10023.